

FRactal ANALYSIS OF AGGREGATES OF NON-UNIFORMLY SIZED PARTICLES: AN APPLICATION TO MACAQUE MONKEY CORTICAL PYRAMIDAL NEURONS

B.I. HENRY

Department of Applied Mathematics, School of Mathematics, University of New South Wales, Sydney NSW 2052, Australia

E-mail: B.Henry@unsw.edu.au

P.R. HOF^{A,B,C}, P. ROTHNIE^{D,C} AND S.L. WEARNE^{D,B,C}

^A *Kastor Neurobiology of Aging Laboratories,*

^B *Fishberg Research Center for Neurobiology,*

^C *Computational Neurobiology and Imaging Center,*

^D *Department of Biomathematical Sciences,*

Mount Sinai School of Medicine, New York, New York, 10029-6574

E-mail: patrick.hof@mssm.edu, paul@camelot.mssm.edu, susan@camelot.mssm.edu

A variant of the cumulative mass method is developed for measuring the multi-fractal dimension spectrum of three-dimensional aggregates composed of particles of different sizes. The method is applied to measuring the mass fractal dimensions of pyramidal neurons of the prefrontal cortex of macaque monkeys, digitized with standard 3-dimensional tracing software. Fractal dimension estimates obtained from our approach are found to be useful for distinguishing two functionally different neuronal types which are visually similar.

Short title: *Fractal Analysis of Pyramidal Neurons*

PACS numbers: 05.40.+j, 68.70.+w

1 Introduction

Measurements of fractal dimensions for geometric or mass multifractals can be obtained from the box counting method or the cumulative mass method¹. The cumulative mass method is particularly popular in applications because it can provide reliable estimates of fractal dimensions for smaller cluster sizes than the box-counting dimension. The cumulative mass method has been used extensively in the fractal analysis of clusters grown using computer growth models such as diffusion-limited aggregation^{1,2,3,4}, in which the growing aggregates are composed of identical sized particles. The cumulative mass method has also been employed in the fractal analysis of neuronal morphology^{5,6,7,8}. In these studies, neuronal morphology has been represented as digitized camera lucida images which can again be regarded as aggregates comprising identical sized particles (pixels). Computer-assisted digitization is increasingly becoming the preferred method of capturing neuronal morphology for geometric and morphometric analysis. Standard 3-D digitization software represents dendritic branches as consecutive cylinders of varying length and diameter, which at high resolution suffer information loss if converted to pixel images in 2-D, and are computationally too demanding to convert to high resolution voxel images in 3-D.

In Section 2 of this paper we introduce a variant of the cumulative mass method

that can be employed in the fractal analysis of aggregates composed of particles of different sizes. In Section 3 we explore an application of this method to the fractal analysis of two different types of macaque monkey cortical pyramidal neurons represented as sequential cylinder segments. The neurons investigated comprise two functional types: those furnishing long corticocortical pathways and those projecting locally, forming short-range networks⁹. The former typically support the transmission of information along hierarchies of organized cortical regions, linking distant and functionally different areas of the cerebral cortex, whereas the latter subserve lattices of connections within a given cortical region. Long corticocortically projecting neurons thus support the transfer of increasingly complex sensory or motor information while short projecting neurons may enable local binding of the converging information within a given cortical domain¹⁰. Although the neurons that constitute these functionally distinct pathways share a general pyramidal morphology, subtle differences in the complexity of their dendritic arbors are yet to be elucidated. Morphometric factors such as mass, branching structure, dendritic taper and rate of change of mass and surface area with distance from the soma are known to affect dendritic integration^{11,12,13,14} and the efficacy of action potential backpropagation¹⁵, which is crucial in synaptic plasticity. Because standard 3-D digitization procedures cannot capture fine dendritic varicosities and spine morphology, which are basic determinants of perimeter complexity, in this study we have concentrated on mass measures of fractal dimension. The application of the cumulative mass method to the fractal analysis of these neurons in this paper is an important first step. The results of our analysis are summarized in Section 4 where we report that mass fractal dimension estimates from the cumulative mass method provide a useful discriminant between short projecting neurons and long projecting neurons. The paper concludes with a discussion in Section 5.

2 Cumulative Mass Method for Non-Uniformly Sized Particles

The cumulative mass method was originally introduced¹ to measure the multifractal dimension spectrum for aggregates consisting of uniform sized particles. Consider a cluster of overall size L comprising N particles each of size a . Cover the cluster with boxes of size l , where $a \ll l \ll L$. Let $M_i(l)$ be the mass of particles in the i th box of size l , and M_0 be the total mass of the cluster. The generalized dimensions are defined by the scaling relation

$$\sum_i \left(\frac{M_i(l)}{M_0} \right)^q \sim \left(\frac{l}{L} \right)^{(q-1)D_q}, \quad (1)$$

where the sum over i is a sum over all boxes that contain particles. The finite particle size a and the finite cluster size L provide lower and upper cut-off length scales for the scaling relation. By considering the quantity

$$p_i(l) = \frac{M_i(l)}{M_0}$$

as a probability distribution, Vicsek and colleagues¹ rewrote the left hand side of Eq.(1) as

$$\sum_i \left(\frac{M_i(l)}{M_0} \right)^q = \frac{\sum_i \left(\frac{M_i(l)}{M_0} \right)^{q-1} \left(\frac{M_i(l)}{M_0} \right)}{\sum_i \left(\frac{M_i(l)}{M_0} \right)} = \left\langle \left(\frac{M_i(l)}{M_0} \right)^{q-1} \right\rangle.$$

The above ensemble average is taken with respect to the normalized probability distribution $p_i(l) = \frac{M_i(l)}{M_0}$, the probability that a randomly chosen particle in the cluster is inside the i th box of size l . Since an average over the lattice boxes with respect to the probability distribution $\frac{M_i(l)}{M_0}$ is equivalent to an average over randomly selected centres, the scaling relation

$$\left\langle \left(\frac{M_i(l)}{M_0} \right)^{q-1} \right\rangle \sim \left(\frac{l}{L} \right)^{(q-1)D_q}$$

will hold when the averaging is made with respect to a uniform probability distribution over the fractal. In the application to growing aggregates this scaling relation is implemented as

$$\left\langle \left(\frac{M(R)}{M_0} \right)^{q-1} \right\rangle \sim \left(\frac{R}{L} \right)^{(q-1)D_q} \quad (2)$$

where $M(R)$ is the mass contained in a ball of size R surrounding a randomly selected particle of the aggregate within the radius of gyration.

Reliable estimates for the mass fractal dimension can be obtained using this approach based on about 10% of the aggregate particles as centres². As an aside we note that the application of this formalism to neuronal morphology in reference⁸ incorrectly uses the exponent q on the left hand side of Eq.(2) rather than the exponent $(q - 1)$.

An average over randomly selected particles is inappropriate for aggregates comprising non-uniformly sized particles. Instead it is necessary to sum over all possible particles taking the different masses of the particles into account. First note that if all particles do have equal mass, then an average over randomly selected particles is equivalent to an average over all particles, so that we can write

$$\frac{1}{N} \sum_{j=1}^N \left(\frac{M_j(R)}{M_0} \right)^{q-1} \sim \left(\frac{R}{L} \right)^{(q-1)D_q}. \quad (3)$$

Now taking the mass of each particle into account (and restricting the sum to particles within the radius of gyration where the scaling laws should persist) we have

$$\sum_{k=1}^{\hat{N}_G} \left(\frac{\hat{M}_k}{M_G} \right) \left(\frac{M_k(R)}{M_0} \right)^{q-1} \sim \left(\frac{R}{R_G} \right)^{(q-1)D_q}. \quad (4)$$

In this equation R_G is the radius of gyration, \hat{N}_G is the number of particles inside R_G , \hat{M}_k is the mass of the k th such particle, M_G is the total mass inside R_G and $M_k(R)$ is the total mass inside a ball of radius R centred on the centre of the k th

particle. The dimensions D_q can be obtained from the straight line slopes in a log-log plot of the scaling relation, Eq.(4), using balls of size R in the range $r < R < R_G$ where r is the size of the largest particle in the cluster. Following¹ we define the cumulative mass dimension of order q for non-uniformly sized particle aggregates as

$$D_q = \frac{1}{q-1} \frac{\log \left[\sum_{k=1}^{\hat{N}_G} \left(\frac{\hat{M}_k}{M_G} \right) \left(\frac{M_k(R)}{M_0} \right) \right]}{\log \left(\frac{R}{R_G} \right)} \quad (5)$$

for R in the range $r < R < R_G$. The mass fractal dimension, D_m , for non-uniformly size particle aggregates is then defined by Eq.(5), with $q = 2$, i.e., $D_m = D_2$. In practical applications the dimensions D_q defined by this equation may not be constant over the full range $r < R < R_G$ and so estimates of D_q from the slopes of straight line portions in log-log plots are employed. An obvious shortcoming in applying Eq.(4) directly is that it is an approximate scaling relation which assumes among other things that: i) any particle with its centre inside a ball of radius R is fully contained within that ball, and ii) the mass scaling in balls centred on the centres of particles is the same as the mass scaling in balls centred on other points of the same particle. If each particle is homogeneous, these two shortcomings can be reduced by replacing each large particle by a cluster of smaller particles with equivalent total mass and occupying approximately the same volume. In the next section we demonstrate this procedure in replacing cylinder segments by equivalent chains of spheres.

3 Fractal Analysis of Pyramidal Neurons

3.1 Data Acquisition

Materials from four adult male long-tailed macaque monkeys (*Macaca fascicularis*, 10-12 years old) were used in the present study. All experimental protocols were conducted within the NIH guidelines for animal research and were approved by the Institutional Animal Care and Use Committee (IACUC) at Mount Sinai School of Medicine. These animals received intracortical injections of the retrograde tracer Fast Blue (Molecular Probes, Eugene, OR; 4% aqueous solution) in area 46 of the prefrontal cortex to identify projection neurons as previously described⁹. The animals were then perfused transcardially under deep anaesthesia⁹, with cold 1% paraformaldehyde in phosphate-buffered saline (PBS) and then for 14 minutes with cold 4% paraformaldehyde in PBS. Following perfusion, 4 mm-thick blocks were dissected out of area 46 and the superior temporal cortex, postfixed for 2 hours in 4% paraformaldehyde, and cut at 400 μm on a Vibratome. For intracellular injection of corticocortically-projecting neurons, these sections were immersed in PBS. Fast Blue-containing neurons were identified under epifluorescence with a UV filter, impaled, and loaded with 5% Lucifer Yellow (Molecular Probes). Neurons were subsequently traced and reconstructed three-dimensionally at 100x magnification using a computer-assisted morphometry system consisting of a Zeiss Axiophot photomicroscope equipped with a Zeiss MSP65 computer-controlled motorized stage (Zeiss, Oberkochen, Germany), a Zeiss ZVS-47E video camera system (Zeiss, Thornwood,

NY), a Macintosh 840 AV microcomputer, and custom designed morphometry software (NeuroZoom¹⁶, NeuroGL [Computational Neurobiology and Imaging Center, Mount Sinai School of Medicine, New York]).

3.2 *Cylinders to Chains of Spheres*

The digitized morphologic data described above are available as a set of cylindrical segments of specified diameter and location. The fractal analysis of these data sets can be found by employing the scaling relation, Eq.(4), with each cylinder segment considered as a separate particle. As discussed above, however, while this scaling relation properly accounts for the different masses of the cylinder segments it does not take into account their different volumes. To address this, we replaced each cylinder segment by a chain of uniformly sized spheres, and then used the spheres as individual particles in the scaling analysis.

Consider a given cylinder segment of length L , radius r and end points \vec{x}_a and \vec{x}_b . We wish to replace each cylinder by a chain of n spheres of uniform radius R so that the chain of spheres is the best single line packing approximation to the cylinder, i.e., we wish to satisfy the dual conditions $\pi r^2 L = n \frac{4}{3} \pi R^3$ and $L = 2nR$. It is a simple matter to solve these simultaneous equations from which we deduce the following two cases:

1. $L \leq \sqrt{6}r$:

The cylinder is replaced by a single sphere with centre

$$\vec{x}_c = \frac{\vec{x}_a + \vec{x}_b}{2}$$

and radius

$$R = \left(\frac{3r^2 L}{4} \right)^{\frac{1}{3}} .$$

2. $L > \sqrt{6}r$:

The cylinder is replaced by $n = \lfloor \frac{L}{\sqrt{6}r} \rfloor$ spheres (where $\lfloor x \rfloor$ denotes the greatest integer not exceeding x), with centres

$$\vec{x}_j = \vec{x}_a + \left(\frac{2j-1}{2n} \right) (\vec{x}_b - \vec{x}_a) \quad j = 1, \dots, n$$

and radii

$$R = \left(\frac{3r^2 L}{4n} \right)^{\frac{1}{3}} .$$

Fig. 1 shows a portion of a neuron represented by cylinder segments and the same portion represented by a chain of spheres using the above approach.

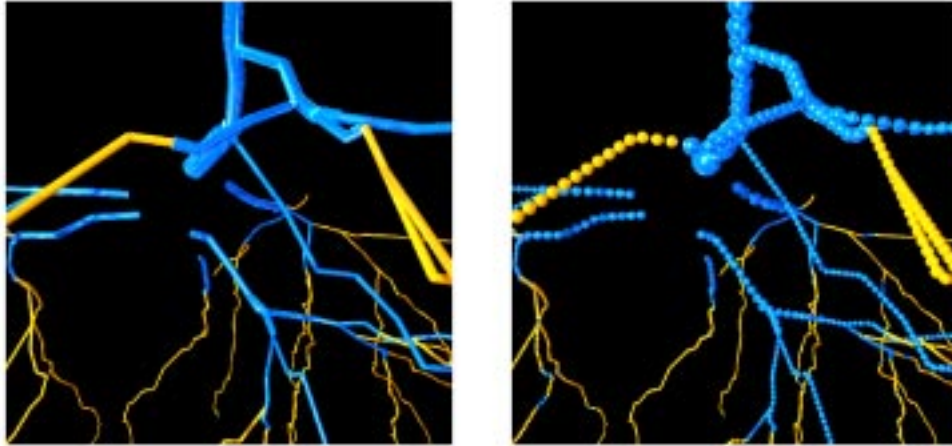


Figure 1. Representation of the same portion of a neuron using cylinder segments (left), and chains of spheres (right).

3.3 Mass Fractal Dimensions

The mass fractal dimensions, D_m , of the neurons are obtained by using the scaling relation, Eq.(4), with $q = 2$, and each cylinder segment replaced by a chain of spheres. The scaling relation is used taking all particle spheres within the radius of gyration as centres for fifty balls of size R uniformly spaced on a log scale in the range $[R_G/8, R_G/2]$. The restriction to the central portion of the neuron within its radius of gyration avoids artefacts associated with the sparsely branching distal regions of the tree. Fig. 2 shows a representative pyramidal neuron and a ball of size R_G centred on the centre of mass of this neuron. It is clear that most of the complexity is contained within this ball. The morphology of the neuron shown in figure 2 and the other pyramidal neurons in this study is characterized by a pyramid-shaped soma, and an overall triangular-shaped dendritic arbor.

The lower ball radius $R_G/8$ used in the scaling analysis was always found to be above the radius of the largest aggregate particle sphere. The slope of the best fit straight line portion in the log-log plots was obtained by identifying the plateau portion in a plot of successive slopes from ten point moving averages. The plateau portion was found to occur towards the upper end of the ball size, $R \approx R_G/2$. Fig. 3(a) shows a log-log plot for a typical neuron; a plot of successive slopes for this neuron using ten point moving averages is shown in Fig. 3(b).

4 Results

Mathematical and statistical analyses were performed using Matlab (The Math-Works, Natick, MA), MAPLE, Fortran90 and C/C++. Neurons were reconstructed

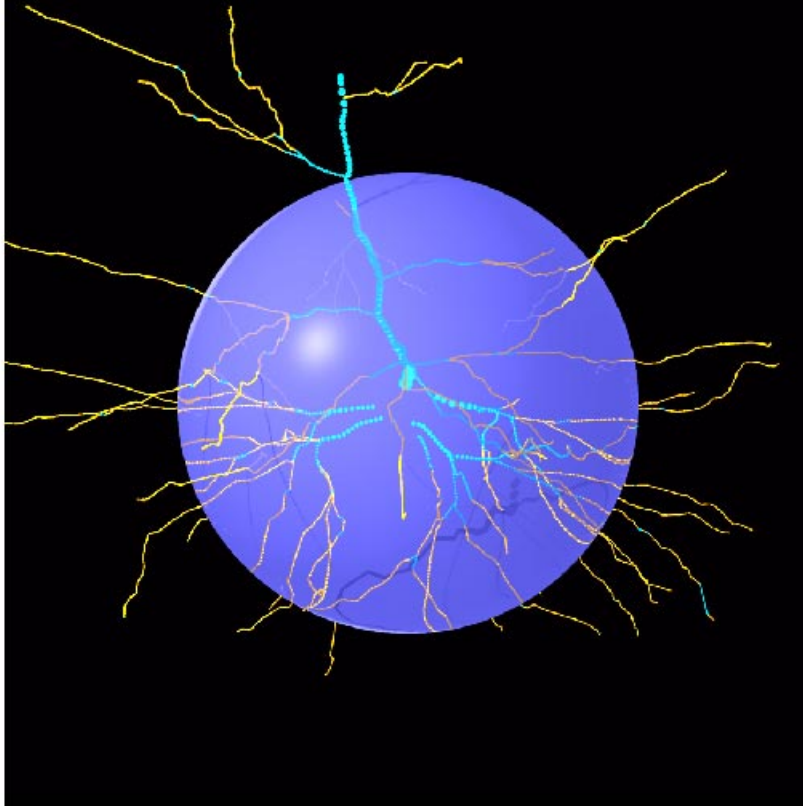


Figure 2. A representative pyramidal neuron shown with a ball of radius equal to the radius of gyration of the neuron which is centred on the centre of mass of the neuron.

and surface rendered in 3-D using custom designed software (NeuroGL). Inspection of relative frequency histograms of D_m revealed that the two neuron classes were approximately normally distributed, and differences between mean values were assessed with t -tests for independent samples. A total of 35 pyramidal cells, comprising 16 long projecting and 19 short projecting neurons from four macaque monkeys were analyzed.

Despite the visual similarity of branching patterns in the two neuron types (compare Fig. 4A and Fig. 4B), the mass fractal dimension D_m was significantly different for the two classes. Short projecting neurons had significantly higher mass dimensions than long (mean D_m for short = 1.62 ± 0.21 s.d.; mean D_m for long =

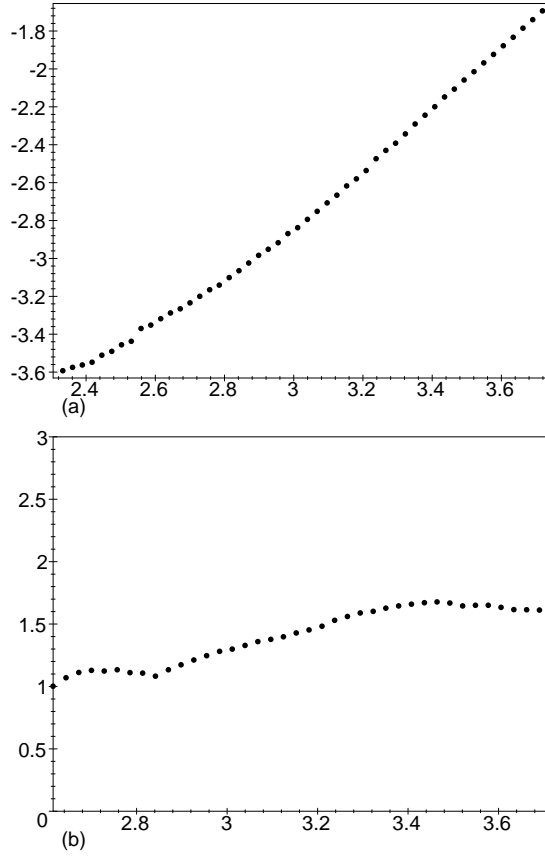


Figure 3. Mass dimension scaling data for a representative pyramidal neuron. The plots show: a) $\log \left[\sum_{k=1}^{N_G} \left(\frac{M_k}{M_G} \right) \left(\frac{M_k(R)}{M_0} \right) \right]$ versus $\log \left[\left(\frac{R}{R_G} \right) \right]$ and b) successive slopes, D_m , from a ten point moving average of the straight line of best fit in this log-log plot.

1.44 ± 0.19 ; $p = 0.0155$), (Table 1). These values for D_m are somewhat higher than values calculated using the 2-D dilation method for pyramidal neurons in macaque monkey¹⁷. However these higher values for D_m are consistent with the generally higher fractal dimensions found using the cumulative mass method as opposed to box-counting or coastline methods^{6,7}.

The calculated mass dimensions associated with the neurons shown in Fig. 4 at first may appear counterintuitive. The long projecting neuron **A** appears slightly more complex than its short projecting counterpart **B**. To elucidate this result, we compared the number of branches originating from the soma, along with the total number of branchpoints, in long and short projecting neurons. Long projecting neurons had significantly more branches (mean 6.25 ± 0.86) than short projecting neurons (mean 5.21 ± 1.08 , $p = 0.0039$). Long neurons also had more branch points (mean 92.13 ± 15.34) than short neurons (mean 72.58 ± 17.71 , $p = 0.0015$). This greater number of branches and branch points compensates visually for the lower

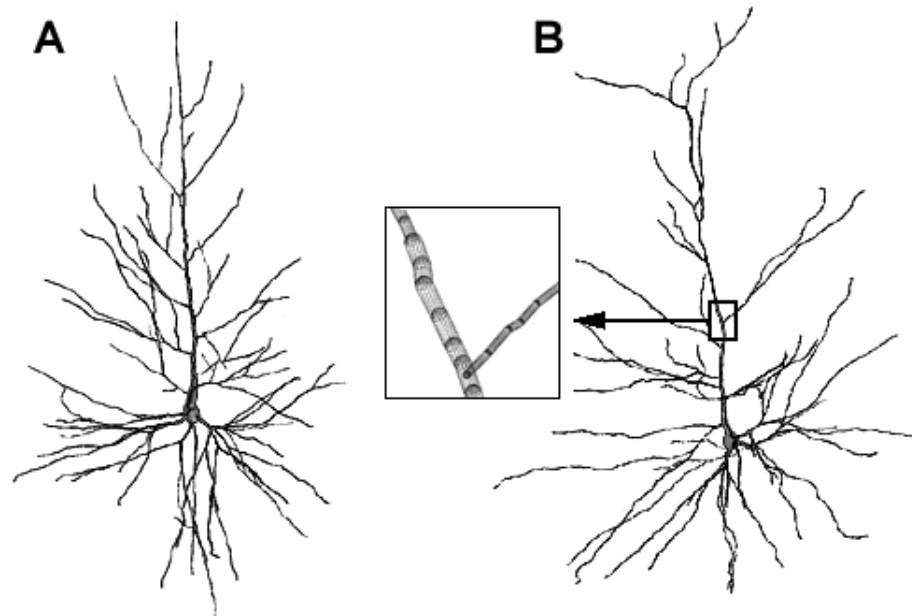


Figure 4. Morphology of two functionally distinct neurons; **A**: long projection neuron and **B**: short projection neuron. The insert shows successive cylinder segments from which the dendritic tree is reconstructed.

rate of increase in mass measured by D_m , increasing the apparent complexity of long projecting neurons relative to short.

| Neuron | N | D_m | S.D. | No. Branches | S.D. | No. Branchpoints | S.D. |
|--------|----|-------|------|--------------|------|------------------|-------|
| Long | 16 | 1.44 | 0.19 | 6.25 | 0.86 | 93.13 | 15.34 |
| Short | 19 | 1.62 | 0.21 | 5.21 | 1.08 | 72.58 | 17.71 |

Table 1. Summary of statistics for long and short projecting neurons. The values in columns 3,5 and 7 represent means for D_m , number of branches, and number of branchpoints, respectively.

5 Discussion

An overall goal of our research is to develop measures of dendritic branching geometry capable of distinguishing functionally relevant morphologic differences that might contribute to variability in neural firing patterns and neuronal plasticity. As

a first step in this direction we have introduced a variant of the cumulative mass method that can be applied to finding multifractal mass dimensions of aggregates of non-uniformly sized particles. This method was then applied to finding the mass fractal dimension of two functionally distinct types of pyramidal neurons. It was found that differences in complexity between long and short projection neurons which are difficult to appreciate by eye (Fig. 4) can nevertheless be discriminated using the mass fractal dimension.

Our results can be contrasted with a recent study comparing 2-D fractal dimensions of pyramidal neurons in different cortical areas of macaque monkey¹⁷, which found that progressively ‘higher order’ cortical neurons had progressively higher fractal dimensions. Using the variant of 3-D mass fractal dimension described in this paper, we find that short projecting neurons, which likely subserve more local information binding within a single cortical domain, had higher values of D_m than long projecting neurons, which link more complex and apparently functionally disparate cortical regions. This result reflects the difference between coastline methods of computing fractal dimension, which measure complexity of the perimeter of an object, and mass methods, which measure the rate at which total mass of the object increases with distance from the center of mass. The rate of increase in mass is directly related to the rate of increase in dendritic surface area with distance from the soma. A recent simulation study examined the correlation between different morphometric parameters and efficiency of forward and backpropagation of action potentials in dendritic arbors with different branching topologies¹⁵. The strongest predictor of propagation failure was the rate of increase in dendritic membrane area with distance from the soma. Functionally, this will result in differences in dendritic integration and synaptic plasticity in neurons with different values of D_m , that are attributable to morphologic variation. As such, D_m represents a valuable independent measure of functionally relevant morphologic differences that are difficult to assess visually.

In future work we plan to investigate the multifractal dimension spectrum as well as detailed branching analysis for these and other neurons.

Acknowledgments

We thank Huiling Duan, Michael Einstein, and Daniil Rolshud for assistance with cell loading and imaging, Douglas Ehlenberger, Kevin Kelliher and Alfredo Rodriguez for technical assistance, and Dr John Morrison for scientific advice. Supported by NIH Grants AG05138, AG06647, MH58911 and DC04632, the Howard Hughes Medical Institute and the Australian Research Council.

References

1. T. Tel, A. Fulop and T. Vicsek, Determination of fractal dimensions for geometrical multifractals, *Physica A*, **159**, 155-166, (1989).
2. T. Vicsek, F. Family and P. Meakin, Multifractal geometry of diffusion-limited aggregates, *Europhys. Letts.*, **12**, 217-222, (1990).
3. C-H Lam, Finite-size effects in diffusion-limited aggregation, *Phys. Rev. E*,

- 52**, 2841-2847, (1995).
4. F. Jestczemski and M. Sernetz, Multifractal approach to inhomogeneous fractals, *Physica A*, **223**, 275-282, (1996).
 5. F. Caserta, H.E. Stanley, W.D. Eldred, G. Daccord, R.E. Hausman and J. Nittman, Physical mechanism underlying neurite outgrowth: A quantitative analysis of neuronal shape, *Phys. Rev. Letts.*, **64**, 95-98, (1990).
 6. F. Caserta, W.D. Eldred, E. Fernandez, R.E. Hausman, L.R. Stanford, S.V. Bulderev, S. Schwarzer and H.E. Stanley, Determination of fractal dimension of physiologically characterized neurons in two and three dimensions, *J. Neurosci. Methods*, **56**, 133-144, (1995).
 7. T.G. Smith Jr., G.D. Lange and W.B. Marks, Fractal methods and results in cellular morphology - dimensions, lacunarity and multifractals, *J. Neurosci. Methods*, **69**, 123-136, (1996).
 8. E. Fernandez, J.A. Bolea, G. Ortega and E. Louis, Are neurons multifractals?, *J. Neurosci. Methods*, **89**, 151-157, (1999).
 9. E.A. Nimchinsky, P.R. Hof, W.G. Young and J.H. Morrison, Neurochemical, morphologic, and laminar characterization of cortical neurons in the cingulate motor areas of the macaque monkey, *J. Comp. Neurol.*, **374**, 136-160, (1996).
 10. P.R. Hof, E.A. Nimchinsky and J.H. Morrison. Neurochemical phenotype of corticocortical connections in the macaque monkey: quantitative analysis of a subset of neurofilament protein-immunoreactive projection neurons in frontal, parietal, temporal, and cingulate cortices, *J. Comp. Neurol.*, **362**, 109-133, (1995).
 11. W. Rall, Theoretical significance of dendritic trees for input-output relations, In: *Neural Theory and Modeling*, R.F. Reiss (Ed.), 73-79, Stanford University Press, Stanford, (1964).
 12. Z.F. Mainen and T.J. Sejnowski, Influence of dendritic structure on firing patterns in model neocortical neurons, *Nature*, **382**, 363-366, (1996).
 13. A. Surkis, C.S. Peskin, D. Tranchina and C.S. Leonard. Recovery of cable properties through active and passive modeling of subthreshold membrane responses from laterodorsal tegmental neurons, *J. Neurophysiol.*, **80**, 2593-2607, (1998).
 14. C. Koch, *Biophysics of Computation: Information Processing in Single Neurons*, Oxford University Press, New York, (1999).
 15. P. Vetter, A. Roth and M. Hausser, Propagation of action potentials in dendrites depends on dendritic morphology, *J. Neurophysiol.*, **85**, 926-937, (2001).
 16. W.G. Young, E.A. Nimchinsky, P.R. Hof, J.H. Morrison and F.E. Bloom, *NeuroZoom Software User Guide and Reference Books*, YBM Inc, San Diego, (1997).
 17. H.F. Jelinek and G.N. Elston, Pyramidal neurones in macaque visual cortex: interareal phenotypic variation of dendritic branching patterns, *Fractals*, **9**, In Press.